Rakenteiden Mekaniikka (Journal of Structural Mechanics)
Vol. 57, No. 1, 2024, pp. 24–36
http://rakenteidenmekaniikka.journal.fi
https://doi.org/10.23998/rm.141576

VERTAISARVIOITU
KOLLEGIALT GRANSKAD
PEER-REVIEWED
www.tsv.fi/tunnus

A thermo-mechanical numerical method for modelling heating due to frictional sliding

Timo Saksala

Summary Heating due to frictional sliding is an important phenomenon in tribological applications. The present study develops a numerical method based on the finite elements (FE) for modelling frictional sliding induced heating. More specifically, the method is designed for applications where the behavior of the tool part of the frictional contact couple is not critical so that it can be idealized as a rigid body. The contact between the tool and the target, assuming linear elastic material, is modelled with the penalty method. The FE-discretized balance of linear momentum is time discretized with the Newmark scheme, and the FE-discretized heat equation is time discretized with the backward Euler scheme. The global coupled thermo-mechanical problem is solved with a globally iterative staggered approach. The frictional contact model is verified against analytical solution of a rotating blade pressed against a plane. Finally, a validation simulation of a pin-on-disc tribology test is carried out.

Key words: finite elements, frictional sliding contact, frictional heating, pin-on-disc test

Received: 28 November 2023. Accepted: 30 January 2024. Published online: 27 March 2024.

Introduction

Frictional sliding induced heating effects cause concern in tribological applications, such as friction clutches and brakes [1,2], machining of metals [3,4,5], and friction stir welding [6]. Moreover, substantial local temperature rise may also occur in fretting contact [7], but the temperature effects seem to be seldom included in fretting analyses, see e.g. [8]. Localized heating may cause alterations in material behavior, such as weakening, and even melting of metals in friction clutches and brakes. Therefore, the ability to predict the temperature effects by numerical modelling is an important asset in the related fields of engineering. This has spurred considerable research efforts focused on developing numerical techniques capable of simulating the thermal effects in frictional sliding, as exemplified in Refs. [2,5,9–15]. Another tribological application involving frictional sliding is abrasive tests, such as the pin-on-disc test and its modifications [16,17]. Predictive numerical modelling of these tests facilitates the planning of experiments and the design of new testing methods and has thus drawn substantial attention [18–23].

The present study develops a numerical approach to predict the heat generation due to frictional sliding. While the works cited above have their merits, the distinct aim of the present study is to develop a platform code capable of being extended to simulate heating due to frictional sliding in any of the mentioned applications. As most of the above cited numerical studies, the present method is also based on the finite element method (FEM). In contrast to these studies, the present method is tailored for applications where the behaviour of the tool is not at the focus of interest so that it can be modelled as a rigid body with virtual geometry. This is many times the case, e.g. in choosing the disc metal alloy in friction brake or clutch design. Another application where the tool behaviour can be neglected (at certain stages of the design process) by describing the tool as a rigid body is the drill bit design, as demonstrated by Saksala [24,25]. Moreover, at this stage of development, linear elastic material is assumed while the focus is on the coupled thermo-mechanical problem with Coulombian frictional contact. The model is finally validated by predicting heat generation in a pin-on-disc test. The method was implemented with Matlab software.

Numerical method

The numerical method for modelling frictional sliding induced heating consists of the material model, a tool-base material interaction model, the heat generation model, and the thermo-mechanical equation system governing the problem and its solution technique.

The base material is assumed to be linear elastic so that the small deformation assumption applies. The constitutive relation can thus be written as

$$\boldsymbol{\sigma} = \mathbf{C}_\mathrm{e} : (\boldsymbol{\varepsilon} - \boldsymbol{\varepsilon}_\theta) \tag{1}$$

$$\boldsymbol{\varepsilon}_\theta = \alpha \Delta\theta \mathbf{I} \tag{2}$$

where the symbol meanings are: $\boldsymbol{\sigma}$ is the stress tensor; $\mathbf{C}_\mathrm{e}$ is the elasticity tensor; $\boldsymbol{\varepsilon}$ is the total strain tensor; $\boldsymbol{\varepsilon}_\theta$ is the thermal strain; α and $\Delta\theta$ are the thermal expansion coefficient and the temperature change; $\mathbf{I}$ is the second order identity tensor.

Tool-base material interaction model

As discussed in Introduction, the tool part of the contact pair is modelled as a rigid body with virtual geometry. Moreover, the interaction of the tool and the base material is modelled by contact mechanics principles [26], as described later. The tool itself is represented by a single node, as illustrated in Figure 1 below. The sliding of the tool on the base material is modelled as a moving set of boundary (surface) nodes.

When the node representing the tool moves (slides), possibly translating with velocity v_0 and/or rotating with angular velocity ω, on the surface of base material, the set of possible contact nodes, marked red in Figure 1, needs to be searched at each time instant. From this set, the nodes truly in contact are then detected and consequently included in the contact force solution and the assembly of the external (frictional) heat flux vector.

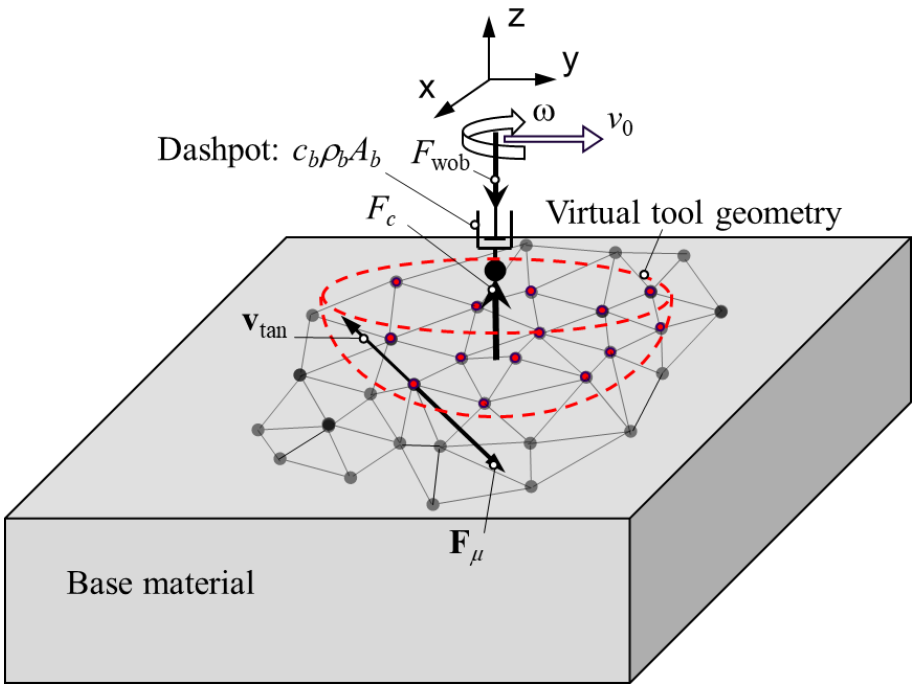

Figure 1. Schematics of tool-base material interaction model.

The viscous damper (dashpot) attached to the tool node absorbs the possible wave effects. To absorb the wave, the damper properties are defined by a computational area A_b of the tool, the density ρ_b, and the bar velocity $c_b = \sqrt{E_b/\rho_b}$ with E_b being the Young's modulus of the tool material.

Furthermore, loading, or the weight on bit, is applied on the tool by F_{wob}, which is balanced by the normal contact force F_{c}. The tool also exerts a friction force, $\mathbf{F}_\mu$, in the direction opposite to the tangential velocity $\mathbf{v}_{\text{tan}}$. The equations of motion for the tool are written as

$$m_b\ddot{u}_{b,z} + c_b\rho_b A_b\dot{u}_{b,z} = F_{wob} + F_c \quad (3)$$

$$m_b\ddot{u}_{b,x} + c_b\rho_b A_b\dot{u}_{b,x} = F_x^\mu \quad (4)$$

$$m_b\ddot{u}_{b,y} + c_b\rho_b A_b\dot{u}_{b,y} = F_y^\mu \quad (5)$$

$$J_b\ddot{\phi}_{b,z} + c_{bs}\rho_b I_b\dot{\phi}_{b,z} = M_\mu,\ M_\mu = \sum_{i=1}^{N_c} F_i^\mu r_i \quad (6)$$

where m_b is a computational mass for the tool, $\ddot{u}_{b,i}$ and $\dot{u}_{b,i}$ are the acceleration and velocity of the tool in i-direction. Moreover, $\ddot{\phi}_{b,z}$ and $\dot{\phi}_{b,z}$ are the angular acceleration and velocity of the tool, J_b and I_b are the computational moment of inertia and polar moment, respectively. Furthermore, c_{bs} is the shear wave velocity, and M_μ is the moment of friction forces F_i^μ with r_i being the orthogonal distance of node i (in contact) from the rotation center. These equations are to be augmented to the global equation of motion described next. However, in practice Equation (6) is not needed as the tool angular velocity, $\dot{\phi}_{b,z} = \omega$, is usually given as a boundary condition and the moment can be calculated based on the friction forces on the base material.

The governing coupled thermo-mechanical equations

The strong or local form of the equations governing the frictional heating can be written as [27,28]

$$\rho\ddot{\mathbf{u}} = \nabla \cdot \boldsymbol{\sigma} + \mathbf{b} \tag{7}$$
$$\rho c\dot{\theta} = -\nabla \cdot \mathbf{q} + Q_{\text{mech}} + q_{\mu} \tag{8}$$
$$\mathbf{q} = -k\nabla\theta,\ q_{\mu} = \eta\mu p_N v_{\text{slip}} \tag{9}$$

The symbols in these equations are: ρ and c are the density and the specific heat capacity of the material; $\dot{\theta}$ is the rate of change of temperature; $\ddot{\mathbf{u}}$ is the acceleration vector; $\mathbf{b}$ is the volume force; $\mathbf{q}$ is the heat flux vector related to temperature gradient $\nabla\theta$ and the conductivity k by the Fourier's law; Q_{mech} expresses the mechanical heat production through plastic dissipation and elastic strain rate. These sources of heat are ignored so that $Q_{\text{mech}} \equiv 0$ (see the justification in [29]); q_{μ} is the heat flux density due to frictional sliding; η is a parameter controlling the fraction of heat going to the base ($1-\eta$ then goes to the tool); μ is the Coulomb friction coefficient; p_N is the contact pressure; v_{slip} is the relative tangential velocity between to contacting bodies. It should be noted that only slip condition is considered in the present approach. Then, the boundary conditions can be expressed as

$$\boldsymbol{\sigma} \cdot \mathbf{n}_{\Gamma} = \hat{\mathbf{t}} \ \text{ on } \Gamma_{\sigma} \tag{10}$$
$$\mathbf{u} = \hat{\mathbf{u}} \ \text{ on } \Gamma_{u} \tag{11}$$
$$g_N \geq 0,\ p_N \leq 0,\ g_N p_N = 0 \ \text{ on } \Gamma_c \tag{12}$$
$$\mathbf{t}_T = -\mu p_N \frac{\mathbf{v}_{\text{rtan}}}{\|\mathbf{v}_{\text{rtan}}\|} \ \text{ on } \Gamma_c \tag{13}$$

where the notation meanings are as follows: $\hat{\mathbf{t}}$, $\hat{\mathbf{u}}$ are the prescribed surface traction and displacement, defined on their respective parts Γ_{σ} and Γ_{u} of the boundary Γ; $\boldsymbol{n}_{\Gamma}$ is the surface normal on Γ_{σ}; $g_N = \mathbf{u}_{\text{bit}} \cdot \mathbf{n}_{\text{bit}} + \mathbf{u}_{\text{base}} \cdot \mathbf{n}_{\text{base}}$ is the normal gap function where $\mathbf{u}_{\text{bit}}$, $\mathbf{n}_{\text{bit}}$ and $\mathbf{u}_{\text{base}}$, $\mathbf{n}_{\text{base}}$ are the displacement vectors and the outer normal vectors of the bit (tool) and the base material, respectively, on the contact part of the surface Γ_c; $\mathbf{t}_T$ is the (Coulombian) friction traction due to slip or relative tangential velocity $\mathbf{v}_{\text{rtan}}$. In order to solve Equations (7) and (8) in time, initial conditions must be defined for displacement, velocity, and temperature: $\mathbf{u}(\mathbf{x},0) = \mathbf{u}_0(\mathbf{x})$, $\dot{\mathbf{u}}(\mathbf{x},0) = \dot{\mathbf{u}}_0(\mathbf{x})$, $\theta(\mathbf{x},0) = \theta_0(\mathbf{x})$.

FE discretized system of equations and its solution

The finite element discretized version of the equations above can be derived by the standard steps using the principle of virtual work [26,27]. When the penalty method is used to impose the contact constraints, the equations of motion and thermal balance written at time $t + \Delta t$ are:

$$\mathbf{M}\ddot{\mathbf{u}}_{t+\Delta t} + \mathbf{C}\dot{\mathbf{u}}_{t+\Delta t} + \mathbf{K}\mathbf{u}_{t+\Delta t} = \mathbf{f}^{\text{ext}}_{t+\Delta t} + \mathbf{K}_{u\theta}(\boldsymbol{\theta}_{t+\Delta t} - \boldsymbol{\theta}_0) + \\ + p\mathbf{G}^{\mathrm{T}}(\mathbf{G}\mathbf{u}_{t+\Delta t} - \mathbf{b}) + \mathbf{f}_{\mu,t+\Delta t} \quad (14)$$

$$\mathbf{C}_\theta\dot{\boldsymbol{\theta}}_{t+\Delta t} + (\mathbf{K}_\theta + \mathbf{K}_{\mathrm{h}})\boldsymbol{\theta}_{t+\Delta t} = \mathbf{f}_{\mu\theta,t+\Delta t}(\dot{\mathbf{u}}, \mathbf{f}_\mu) + \mathbf{f}_{h,t+\Delta t} \quad (15)$$

where $\mathbf{M}$ is the mass matrix; $\mathbf{C}$ is the damping matrix related to the dashpot in Equation (3)–(5); $\mathbf{K}$ is the stiffness matrix; $\mathbf{C}_\theta$ is thermal capacity matrix; $\mathbf{K}_\theta$ is the thermal conductivity matrix; $\mathbf{u}$, $\dot{\mathbf{u}}$ and $\ddot{\mathbf{u}}$ are the nodal displacement, velocity and acceleration, respectively; $\boldsymbol{\theta}$ and $\dot{\boldsymbol{\theta}}$ are the nodal temperature vector and its rate; p is the penalty parameter; $\mathbf{G}$ is the normal contact constraint matrix so that for each contact pair i, $G_{ij}u_j = g_N$ is the normal gap; $\mathbf{b}$ is the initial distance between all the potential contact nodes on the base material and the tool; $\mathbf{K}_{\mathrm{h}}$ and $\mathbf{f}_{\mathrm{h}}$ are the contributions from boundary convection; $\mathbf{K}_{u\theta}$ is the displacement-temperature coupling matrix arising from the constitutive Equation (1); $\mathbf{f}^{\text{ext}}$ is the external nodal force vector related to the weight on bit force F_{wob} in Figure 1; $\mathbf{f}_{\mu\theta}$ is the heat source due to frictional sliding; $\mathbf{f}_\mu$ is the friction force vector. These are further defined as follows:

$$\mathbf{M} = \mathbf{A}_{e=1}^{N_{\text{el}}} \int_{V_e} \mathbf{N}_e^{\mathrm{T}}\mathbf{N}_e \, \mathrm{d}V, \ \mathbf{C} = c_b\rho_b A_b \mathrm{diag}([\mathbf{I}_{\text{bit}}, \mathbf{0}]) \quad (16)$$

$$\mathbf{K} = \mathbf{A}_{e=1}^{N_e} \int_{V_e} \mathbf{B}_u^{e,\mathrm{T}}\mathbf{C}_e\mathbf{B}_u^e \mathrm{d}V\,, \quad \mathbf{K}_{u\theta} = \mathbf{A}_{e=1}^{N_e} \int_{V_e} \alpha\mathbf{B}_u^{e,\mathrm{T}}\mathbf{C}_e[\mathbf{1} \otimes \mathbf{I}_\theta]\mathrm{d}V \quad (17)$$

$$\mathbf{C}_\theta = \mathbf{A}_{\mathrm{e}=1}^{N_{\mathrm{e}}} \int_{V_{\mathrm{e}}} \rho c\mathbf{N}_\theta^{\mathrm{e},\mathrm{T}}\mathbf{N}_\theta^{\mathrm{e}}\mathrm{d}V, \quad \mathbf{K}_\theta = \mathbf{A}_{\mathrm{e}=1}^{N_{\mathrm{e}}} \int_{V_{\mathrm{e}}} k\mathbf{B}_\theta^{\mathrm{e},\mathrm{T}}\mathbf{B}_\theta^{\mathrm{e}}\mathrm{d}V \quad (18)$$

$$\mathbf{K}_{\mathrm{h}} = \mathbf{A}_{\mathrm{e}=1}^{N_{\mathrm{fh}}} \int_{A_{\mathrm{e}}} h\mathbf{N}_\theta^{\mathrm{e},\mathrm{T}}\mathbf{N}_\theta^{\mathrm{e}}\mathrm{d}A\,, \quad \mathbf{f}_h = \mathbf{A}_{\mathrm{e}=1}^{N_{\mathrm{fh}}} \int_{A_{\mathrm{e}}} h\theta_a\mathbf{N}_\theta^{\mathrm{e},\mathrm{T}}\,\mathrm{d}A \quad (19)$$

$$\mathbf{f}_{\mu,t+\Delta t} = -\sum_{nd=1}^{N_{\text{conts}}} \mu F_N^{nd} \frac{\mathbf{v}_{\tan,nd}}{\|\mathbf{v}_{\tan,nd}\|} \quad (20)$$

$$\mathbf{f}_{\mu\theta,t+\Delta t} = \mathbf{A}_{e=1}^{N_{\text{fc}}} \int_{A_e} q_{\mu,t+\Delta t}\mathbf{N}_\theta^{e,\mathrm{T}}\,\mathrm{d}A, \ q_{\mu,t+\Delta t} = \eta\mu\bar{F}^e_{N,t+\Delta t}/(3A_{ef})\|\mathbf{v}_{\tan,t+\Delta t}\| \quad (21)$$

In these equations: $\mathbf{A}$ is the standard finite element assembly operator; V_e is the volume of an element; A_e is the area of an element facet; N_e is the number of elements; In $(16)_2$, diag means that a diagonal matrix is formed from the argument, and $\mathbf{I}_{\text{bit}} = [1\ 1\ 1]$; $\mathbf{B}_u^e$ in (17) is the gradient of the interpolation matrix $\mathbf{N}_e$ for the displacement; $\mathbf{N}_\theta^{\mathrm{e}}$ is the temperature interpolation matrix; $\mathbf{B}_\theta$ is the gradient (matrix) of $\mathbf{N}_\theta$; In (19), h and θ_a are the convection coefficient and the ambient temperature; N_{fh} is the number of elements with a facet on the boundary where the convection BC is defined; In $(17)_2$, α is the thermal expansion coefficient, and in $\mathbf{1} \otimes \mathbf{I}_\theta$, $\mathbf{1}$ is the Voigt version of the second order unit tensor and $\mathbf{I}_\theta$ is a special operator which gives the average of the temperature at the nodes of a finite element; The friction force vector $\mathbf{f}_\mu$ in (20) is calculated as a sum for N_{conts} active contact nodes with μ being the friction coefficient, F_N^{nd} the normal contact force for node nd, and $\mathbf{v}_{\tan,nd}$ the relative tangential velocity (slip), equivalent to $\mathbf{v}_{\text{rtan}}$ in Equation (13), at the same node; q_μ in (21) is the discretized counterpart of $(9)_2$ so that $p_N = \bar{F}_N^e/(3A_{ef})$, where A_{ef} is the area of the finite element face (which count N_{fc} in total) on the contact surface and $\bar{F}_N^e$ is the sum of the nodal forces over that face; $\|\mathbf{v}_{\tan,t+\Delta t}\|$ is corresponds to v_{slip} in $(9)_2$.

The equation of motion (14) of the spatially (FE) discretized coupled system is further discretized in time by the Newmark scheme [30]:

$$\dot{\mathbf{u}}_{t+\Delta t} = \dot{\mathbf{u}}_t + (1-\gamma)\Delta t\ddot{\mathbf{u}}_t + \gamma\Delta t\ddot{\mathbf{u}}_{t+\Delta t} \tag{22}$$

$$\mathbf{u}_{t+\Delta t} = \mathbf{u}_t + \Delta t\dot{\mathbf{u}}_t + \left(\frac{1}{2}-\beta\right)\Delta t^2\ddot{\mathbf{u}}_t + \beta\Delta t^2\ddot{\mathbf{u}}_{t+\Delta t} \tag{23}$$

which is here applied in the unconditionally stable midpoint rule, i.e. β = 1/4, γ = 1/2. Moreover, the implicit backward Euler scheme is used to convert the rate of change of temperature in (15) to its algorithmic counterpart $\dot{\boldsymbol{\theta}}_{t+\Delta t} = (\boldsymbol{\theta}_{t+\Delta t} - \boldsymbol{\theta}_t)/\Delta t$. Applying these schemes to (14) and (15) leads to the algebraic equations for solving the unknown fields $\mathbf{u}_{t+\Delta t}$ and $\boldsymbol{\theta}_{t+\Delta t}$. However, while the heat balance equation is linear in the present case, the equation of motion is nonlinear due to contact constraints. The staggered approach based on the isothermal split [27] is chosen here to solve the coupled system of algebraic equations. The effective stiffness matrix for the iterative solution of the equation of motion is

$$\widehat{\mathbf{K}}_{\tan} = \mathbf{K} + \tfrac{1}{\beta^2}\mathbf{M} + \tfrac{\gamma}{\beta\Delta t}\mathbf{C} + p\mathbf{G}^T\mathbf{G} \tag{24}$$

The iterative (for displacement) staggered algorithm can now be presented as:

1. Solve: $(\mathbf{C}_\theta + \Delta t\mathbf{K}_\theta)\boldsymbol{\theta}_{t+\Delta t} = \mathbf{C}_\theta\boldsymbol{\theta}_t + \Delta t\mathbf{f}_{\mu\theta,t+\Delta t}(\dot{\mathbf{u}}_t) \rightarrow \boldsymbol{\theta}_{t+\Delta t}$
2. Predict: $\dot{\tilde{\mathbf{u}}}^0_{t+\Delta t} = \dot{\mathbf{u}}_t + (1-\gamma)\Delta t\ddot{\mathbf{u}}_t,\ \tilde{\mathbf{u}}^0_{t+\Delta t} = \mathbf{u}_t + \Delta t\dot{\mathbf{u}}_t + \left(\frac{1}{2}-\beta\right)\Delta t^2\ddot{\mathbf{u}}_t$

Calculations for iteration *n*: While $\Delta u_{rel} > TOL$ do

3. Solve: $\widehat{\mathbf{K}}^n_{\tan}\mathbf{u}^{n+1}_{t+\Delta t} = \mathbf{f}^n_{\text{tot}}(\boldsymbol{\theta}_{t+\Delta t}) \rightarrow \mathbf{u}^{n+1}_{t+\Delta t}$
   $\mathbf{f}^n_{\text{tot}} = \mathbf{K}_{u\theta}(\boldsymbol{\theta}_{t+\Delta t} - \boldsymbol{\theta}_0) + \mathbf{f}^{\text{ext}}_{t+\Delta t} + p\mathbf{G}^{\text{T}}\mathbf{b} + \mathbf{f}^n_{\mu,t+\Delta t} - \mathbf{C}\dot{\tilde{\mathbf{u}}}^n_{t+\Delta t} + \left(\frac{1}{\beta^2}\mathbf{M} + \frac{\gamma}{\beta\Delta t}\mathbf{C}\right)\tilde{\mathbf{u}}^n_{t+\Delta t}$
4. Calculate acceleration and update velocity:
   $\ddot{\mathbf{u}}^{n+1}_{t+\Delta t} = \frac{1}{\beta\Delta t^2}(\mathbf{u}^{n+1}_{t+\Delta t} - \tilde{\mathbf{u}}^n_{t+\Delta t}),\ \dot{\mathbf{u}}^{n+1}_{t+\Delta t} = \dot{\tilde{\mathbf{u}}}^n_{t+\Delta t} + \gamma\Delta t\ddot{\mathbf{u}}^{n+1}_{t+\Delta t}$
5. Calculate the relative change: $\Delta u_{rel} = \left\|\mathbf{u}^{n+1}_{t+\Delta t} - \tilde{\mathbf{u}}^n_{t+\Delta t}\right\| / \|\tilde{\mathbf{u}}^n_{t+\Delta t}\|$.
   Set $\tilde{\mathbf{u}}^{n+1}_{t+\Delta t} = \mathbf{u}^{n+1}_{t+\Delta t}$, $n = n+1$ and go to 3.

It is clear from the structure of this algorithm that the iteration for the new displacement field is not in the typical form used with nonlinear equations, which usually involves linearization of the nonlinear equation of motion and using its fulfillment in the stopping criteria while solving for the displacement increment $\Delta\mathbf{u}$ (as in the Newton-Raphson method), not the total displacement as here. However, here the equation of motion is linear in material behavior, and geometrically linear due to the small deformation framework, while the only nonlinearity comes from the contact formulation. Hence, this form of iteration solving for the total displacement in Step 3 is justified. It should also be noted that new contacts need to be found and the matrix $\mathbf{G}$ as well as the heat source vector, $\mathbf{f}_{\mu\theta}$, assembled at each time step. Finally, the linear system in Step 1 is solved with the Matlab backslash operation while the larger system in Step 3 is solved with the stabilized bi-conjugate gradient method using the incomplete LU-factorization as a preconditioner.

Numerical examples

The numerical method is now first verified with an analytical solution for the normal contact force and friction moment during rotational-frictional sliding. Then the method is validated in simulations of heat generation in a pin-on-disc test on a friction material.

Model verification with an analytical solution for friction moment

Consider a blade (width w, length $2R$) pressed with pressure p against a plane schematically described in Figure 2. The blade is rotating with a constant angular velocity ω, and the coefficient of friction between the blade and the plane is μ.

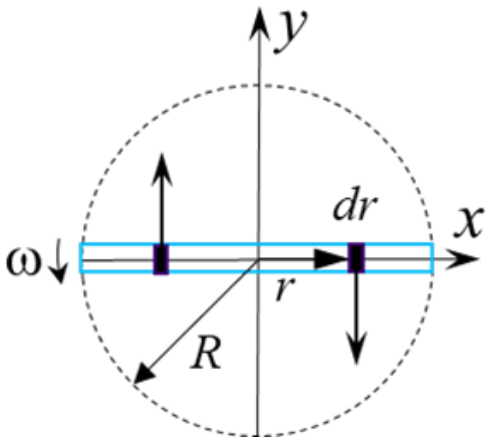

Figure 2. Schematic of a rectangular blade with a length of $2R$ and width of w rotating with a constant angular velocity ω while pressed against the xy-plane.

The moment due to friction, M_μ, can be solved analytically as follows:

$$M_\mu = \int_A dM = \int_A \mu p r dA = 2\mu \frac{F_N}{2Rw} w \int_0^R r dr = \mu F_N R/2 \tag{25}$$

where F_N is the normal force. This solution is now exploited for verification of the present method. However, the temperature effects are ignored here, i.e. the frictional heating is not considered.

The application parameters are: R = 4.25 mm; μ = 0.4; ω = 200 RPM; w = 0.5 mm; F_N = 196 N. The relevant model parameters are as follows: Young's modulus E = 30 GPa; Poisson's ratio ν = 0.2; Material density ρ = 2400 kg/m^3; m_b = 0.005 kg; $A_b = \pi R^2$ = 56.75 mm^2; ρ_b = 7800 kg/m^3; E_b = 210 GPa. Finally, the penalty parameter is set to p = 1×10^6 – a value found by trial. Moreover, the time step is set so that the blade rotates one degree 1° during a single time step. The set of contact nodes is updated at each time step. The finite element mesh representing the plane is shown in Figure 3a. It consists of 27257 linear tetrahedrons (16539 degrees of freedom) with a strong refinement at the contact area. An example of simulation results along with the used finite element mesh are shown in Figure 3b-d. It should be noted that the blade rotates counterclockwise.

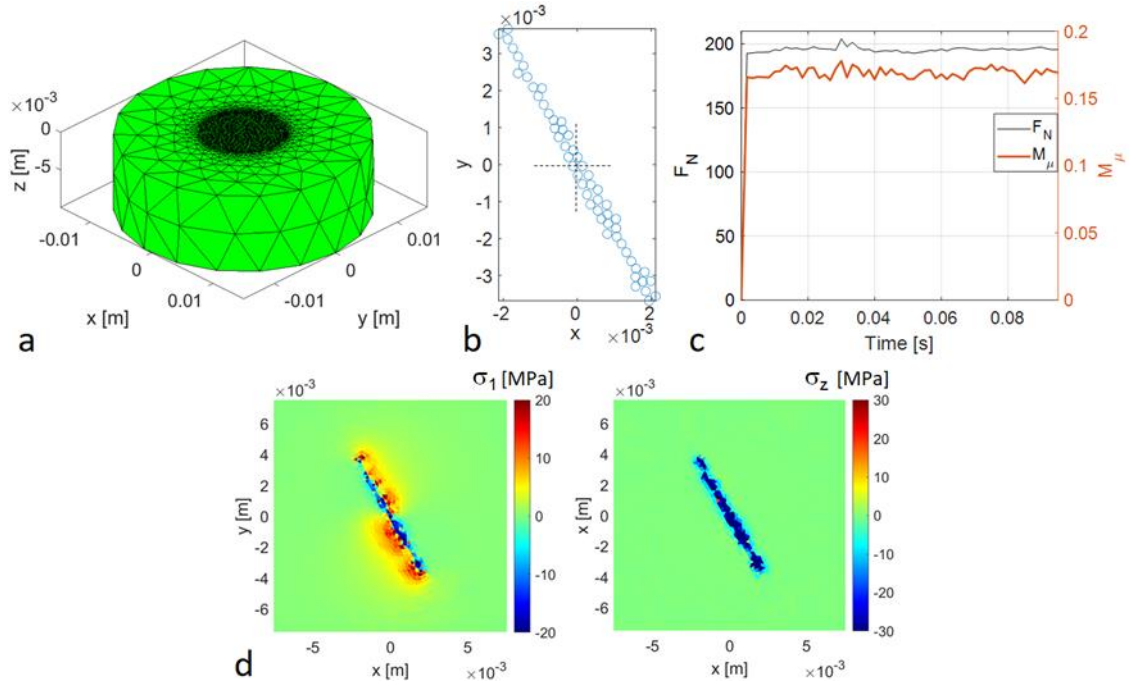

Figure 3. Example of simulation results for the rotational-frictional sliding at t = 0.1 s (α = 2.078 rad): Finite element mesh with 27257 linear tetrahedrons (a); The contact node set (b); The predicted normal force and the friction moment as a function of time (c); The stress components σ_z and σ_1 (d).

The results in Figure 3c show some oscillations in both the normal force and friction moment (calculated by Equation $(6)_2$). These are due to the nonstructured (irregular) mesh used, which means that the number of contact nodes (see an example in Figure 3b) is not the same at each time step when regular blade shape (rectangle) is used. The first principal stress field in Figure 3d illustrates the effect of frictional sliding inducing tensile stresses behind the trailing edge of the rotating blade.

Table 1. Results of the minimalistic parameter study.

p	F_N [N]	R_{bit}	μ	$M_{\mu teor}$ [Nm]	$M_{\mu model}$ [Nm]	Avrg. Err. [%]
1×10^6	196	4.25	0.4	0.1666	0.1697	1.86
1×10^6	196	**2.125**	0.4	0.0833	0.0867	4.08
1×10^6	196	4.25	**0.3**	0.1250	0.1274	1.92
1×10^6	**98**	4.25	0.4	0.0833	0.0849	1.91
1×10^5	196	4.25	0.4	0.1666	0.1682	0.96
1×10^7	196	4.25	0.4	0.1666	0.1744	4.68

In order to verify the method, a minimalist parameter study was performed by varying the terms in the expression for the friction moment in Equation (25) as well as the penalty parameter. The results are shown in Table 1. The error is averaged over the simulation of half a revolution (180°).

It can be observed in Table 1 that the present method performs with an acceptable accuracy in the engineering sense. The errors, reaching 4 %, can be ascribed to the modelling errors, e.g. the relatively coarse mesh used. It can be observed in Figure 3b that the geometry of the contact node set deviates from the one used to derive the theoretical formula for the friction moment in Equation (25), which does not have the blade thickness w. Moreover, the predicted friction moment is calculated by Eq. (6), i.e. $M_\mu = \sum_{i=1}^{N_c} F_i^\mu r_i$, where N_c is the number of contacts. Better accuracy would probably be obtained by a finer mesh or for a different geometry. Finally, the method is not overly sensitive to the value of the penalty parameter, as can be seen in Table 1.

Model validation against experimental results from a pin-on-disc test

The full model, including the thermal part, is now validated against experimental results from a pin-on-disc test reported by Abdullah and Schlattmann [18]. In this test, a steel pin is pressed against a friction disc, which rotates at constant angular velocity ω, being 150 rad/s in the present case.

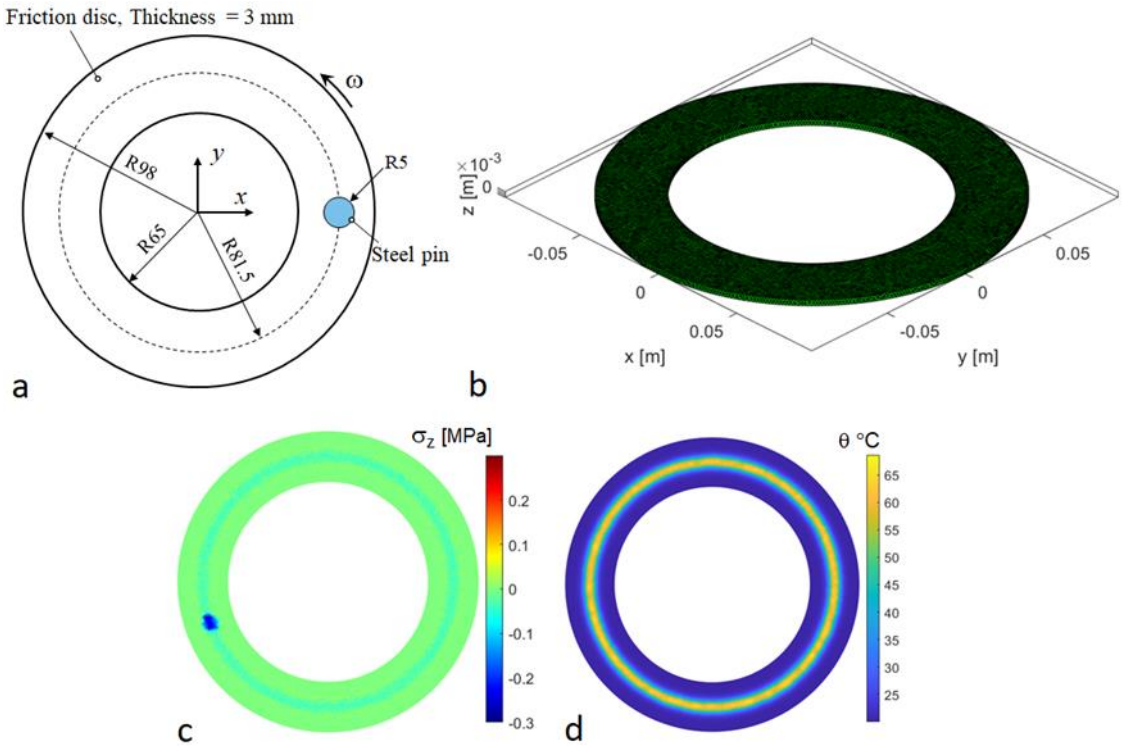

Figure 4. Example of simulation results for the pin-on-disc test at t = 15 s: The schematic for the test (a); The finite element mesh with 80604 linear tetrahedrons (b); The predicted stress component σ_z (c); The predicted temperature distribution (d).

However, in the present modelling approach, the disc is fixed while the node representing the pin moves in the circular trajectory (dashed line) shown in Figure 4a, presenting the schematic principle of the test and the dimensions. The material properties of the friction disc used in the simulation are: Coefficient of friction $\mu = 0.3$; Young's modulus E = 300 MPa; Poisson's ratio $\nu = 0.25$; Material density ρ = 1800 kg/m^3; Thermal expansion coefficient $\alpha = 12\times10^{-6}$ 1/K; Specific heat c = 1000 J/kgK; Thermal conductivity k = 0.65 W/mK. Moreover, the parameter controlling the fraction of heat going to the pin (Equation (9)), η, is set to 0.5, while the penalty coefficient is set to $p = 1\times10^6$. Furthermore, the pressure applied to the pin is p = 0.2 MPa, while the model parameters of the pin are the same as in the above simulations. A convection boundary condition is applied at the top of the disc with the convection coefficient and the ambient temperature being h = 10 W/m^{2}K and θ_a = 293 K. Finally, the time step is the same as in the above simulations. Figure 4b shows the finite element mesh consisting of 80604 linear tetrahedrons (66969 degrees of freedom), and an example of the axial stress component σ_z and the temperature distribution at the end of 15 s simulation are shown in Figure 4c and d.

The temperature reaches 65 °C at some nodes on the disc surface after 15 s of rotation. The comparison to the experimental values at 8, 11, and 15 s is shown in Table 2. It should be mentioned that much higher temperatures (170.6 °C at 15 s) were observed in the steel pin during the experiment [18]. The values in the Table are average temperatures calculated from the data at four locations (x = 81.5 mm, y = 0; x = 0, y = 81.5 mm; x = -81.5 mm, y = 0; x = 0, y = –81.5 mm). Moreover, as the interest of the authors [18] was in the behavior of the pin, they didn't report the exact temperatures on the surface of the friction disc. For present purposes, these were determined from the infrared camera snapshots [18] by image manipulation tools in Matlab.

Table 2. Model predictions vs. experiments for temperature in the pin-on-disc test.

θ_{avrg} [°C]/Time	8 s	11 s	15 s
Experiment	41	47	63
Prediction	43	48	53
Error [%]	4.9	2.1	–15.8

The predicted values differ from the experimental ones with a trend that the at 8 s, the model overshoots the experiment by 4.9 %, but at 15 s underestimation by 15.8 % occurs. The match could possibly be improved by altering some model parameters. However, the agreement is, taking the simplicity of the model into account, acceptable from the engineering point of view. Finally, a note on the convergence of the method is in order. Namely, the relative change of displacement, Δu_{rel}, converged to the set tolerance of 0.001 typically with 5 steps and was very robust.

Conclusions

A numerical method for predicting heating due to frictional sliding was developed in this paper. The method was specifically designed for applications where the behavior of the tool part of the contact pair is not at the focus of interest so that it can be modelled as a rigid body. The finite element discretized coupled thermo-mechanical system was solved with a globally iterative staggered method based on the isothermal split. The frictional contact constraints were handled with the penalty method. As the linear elastic material model and small deformations were assumed, the only nonlinearity in the model comes from the contact constraints.

Thereby, an unconventional iterative solution method was developed for solving the equation of motion discretized in time by the implicit Newmark scheme. In this method, total displacement is solved, as usually with linear equations, instead of the displacement increment, as usually with nonlinear equations. Nevertheless, this approach appeared to be robust and converging relatively fast. Moreover, the present approach predicted the contact force and friction moment generated by a rotating blade with an acceptable accuracy. It also predicted the heating due to frictional sliding in a pin-on-disc test with an engineering-acceptable manner. Therefore, it is concluded that the method is verified (against analytical results) and validated (against experiments).

As such, the method provides a platform for future developments and extensions. For example, nonlinear material models with damage and plasticity can be easily included, after changing the present iterative method to the Newton-Raphson method. Moreover, temperature dependence of the material should be included, especially in applications with intensive heating (friction brakes and clutches). Furthermore, more advanced friction models can be considered when necessary. Finally, even when the tool is modelled as a rigid body, its wear can be accounted for if an empirical wear relation for the tool shape exists, e.g., for blunting of a sharp cutter.

Acknowledgements

The Research Council of Finland is acknowledged for funding this research under Grant Number 340192.

References

[1] Jin Y, Chen L, Cheng, C. Thermal behavior of friction discs in dry clutches based on a non-uniform pressure model. *Case Studies in Thermal Engineering*. 32, 101895, 2022. https://doi.org/10.1016/j.csite.2022.101895

[2] Qiu L, Hong-Sheng Q and Wood A. Two-dimensional finite element analysis investigation of the heat partition ratio of a friction brake. *Proceedings of the Institution of Mechanical Engineers, Part J: Journal of Engineering Tribology*. 232, 1489–1501, 2018. https://doi.org/10.1177/1350650118757

[3] Abukhshim NA, Mativenga PT, Sheikh MA. Heat generation and temperature prediction in metal cutting: A review and implications for high speed machining. *International Journal of Machine Tools and Manufacture*. 46, 782–800, 2006. https://doi.org/10.1016/j.ijmachtools.2005.07.024

[4] Chen L, Tai BL, Chaudhari RG, Song X, Shih AJ. Machined surface temperature in hard turning. *International Journal of Machine Tools and Manufacture*. 121, 10–21, 2017. https://doi.org/10.1016/j.ijmachtools.2017.03.003
[5] Putz M, Schmidt G, Semmler U, Oppermann C, Bräunig M, Karagüzel U. Modeling of Heat Fluxes During Machining and Their Effects on Thermal Deformation of the Cutting Tool. *Procedia CIRP*. 46, 611–614, 2016. https://doi.org/10.1016/j.procir.2016.04.046
[6] Mahakur, V.K., Gouda, K., Patowari, P.K. et al. A Review on Advancement in Friction Stir Welding Considering the Tool and Material Parameters. *Arabian Journal for Science and Engineering*. 46, 7681–7697, 2021. https://doi.org/10.1007/s13369-021-05524-8
[7] Jin, X., Shipway, P.H., Sun, W. The role of frictional power dissipation (as a function of frequency) and test temperature on contact temperature and the subsequent wear behaviour in a stainless steel contact in fretting. *Wear*, 330–331, 103–111, 2015. https://doi.org/10.1016/j.wear.2015.02.022
[8] Mäntylä, A., Juoksukangas, J., Hintikka, J., Frondelius, T., & Lehtovaara, A. FEM-based wear simulation for fretting contacts. *Rakenteiden Mekaniikka*, 53(1), 20–27, 2020. https://doi.org/10.23998/rm.76261
[9] Mamalis AG, Kundrák J., Markopoulos, A. et al. On the finite element modelling of high speed hard turning. *The International Journal of Advanced Manufacturing Technology*. 38, 441–446, 2008. https://doi.org/10.1007/s00170-007-1114-9
[10] Grzesik W, Bartoszuk M, Nieslony P. Finite element modelling of temperature distribution in the cutting zone in turning processes with differently coated tools. *Journal of Materials Processing Technology*. 164–165, 1204–1211, 2005. https://doi.org/10.1016/j.jmatprotec.2005.02.136
[11] Abdullah OI, Schlattmann J. Finite element analysis of temperature field in automotive dry friction clutch. *Tribology in Industry*. 34: 206–216, 2012.
[12] Abdullah OI, Schlattmann J. Thermal behavior of friction clutch disc based on uniform pressure and uniform wear assumptions. *Friction* 4, 228–237, 2016. https://doi.org/10.1007/s40544-016-0120-z
[13] Lee CY, Sup CI, Chai YS. Finite element analysis of an automobile clutch system. *Key Engineering Materials*. 353–358, 2707–2711, 2007. https://doi.org/10.4028/www.scientific.net/KEM.353-358.2707
[14] Dey, A., Rathee, P.S. & Khan, M.M. Computational Fluid Dynamics Approach for Frictional Heat Flow Analysis During Friction Stir Welding Process. *Arabian Journal for Science and Engineering*. 48, 3749–3763, 2023. https://doi.org/10.1007/s13369-022-07215-4
[15] Jedynak, R., Sułek, M. Numerical and Experimental Investigation of Plastic Interaction Between Rough Surfaces. *Arabian Journal for Science and Engineering*. 39, 4165–4177, 2014. https://doi.org/10.1007/s13369-014-1026-6
[16] Kim, D., Kang, H., Song, CH. et al. Design of Pin-on-Disk Type Abrasion Testing Machine for Durability Assessment of Rock Cutting Tools. *International Journal of Precision Engineering and Manufacturing*. 22, 1249–1270, 2021. https://doi.org/10.1007/s12541-021-00534-w
[17] Palanikumar P, Gnanasekaran N, Subrahmanya K, Kaliveeran V. Effect of sliding speed and rise in temperature at the contact interface on coefficient of friction

during full sliding of SS304. *Materials Today: Proceedings*. 27, 1996–1999, 2020. https://doi.org/10.1016/j.matpr.2019.09.046
[18] Abdullah OI, Schlattmann J. Temperature analysis of a pin-on-disc tribology test using experimental and numerical approaches. *Friction*, 4, 135–143, 2016. https://doi.org/10.1007/s40544-016-0110-1
[19] Bartoszuk M, Eddine BMS, Numerical Modelling of Heat Dissipation for the Pin-On-Disc Type Tribometer. *International Journal for Engineering Modelling*. 34, 19–30, 2021. https://doi.org/10.31534/engmod.2021.1.ri.02v
[20] Hegadekatte V, Huber N, Kraft O. Modeling and Simulation of Wear in a Pin on Disc Tribometer. *Tribology Letters*. 24, 51–60, 2006. https://doi.org/10.1007/s11249-006-9144-2
[21] Singh AK, Ranjan V, Tyagi R, Singh BN. Numerical analysis of temperature distribution in sliding contacts of pin on disc model. *Vibroengineering Procedia*. 29, 274–278, 2019. https://doi.org/10.21595/vp.2019.21139
[22] Bortoleto EM, Rovani, Seriacopi AV, Profito FJ, Zachariadis DC, Machado IF, Sinatora A, Souza RM. Experimental and numerical analysis of dry contact in the pin on disc test. *Wear*. 301, 19–26, 2013. https://doi.org/10.1016/j.wear.2012.12.005
[23] Federici, M., Straffelini, G. & Gialanella, S. Pin-on-Disc Testing of Low-Metallic Friction Material Sliding Against HVOF Coated Cast Iron: Modelling of the Contact Temperature Evolution. *Tribology Letters*. 65, 121, 2017. https://doi.org/10.1007/s11249-017-0904-y
[24] Saksala T. Thermal shock assisted percussive drilling: a numerical study on the single-bit axisymmetric case. *International Journal of Rock Mechanics and Mining Sciences*. 132, 104365, 2020. https://doi.org/10.1016/j.ijrmms.2020.104365
[25] Saksala T. 3D Continuum Modelling of PDC Cutting of Rock with a Simple Contact-Erosion Scheme. *Applied Sciences*. 13, 3219, 2023. https://doi.org/10.3390/app13053219
[26] Wriggers, P. Constitutive Equations for Contact Interfaces. In Computational Contact Mechanics; Springer: Berlin/Heidelberg, Germany, 2006.
[27] Ottosen NS, Ristinmaa M. The Mechanics of Constitutive Modeling, Elsevier, 2005.
[28] Abdel-Aal, H.A. Flash Temperature Theory. In: Wang, Q.J., Chung, YW. (eds) Encyclopedia of Tribology. Springer, Boston, MA, 2013. https://doi.org/10.1007/978-0-387-92897-5_1312
[29] Saksala, T., Pressacco, M., Holopainen, S., & Kouhia, R. Numerical modelling of heat generation during shear band formation in rock. *Rakenteiden Mekaniikka*, *52*(2), 53–60, 2019. https://doi.org/10.23998/rm.75287
[30] Hughes TJR. The Finite Element Method: Linear Static and Dynamic Finite Element Analysis. Prentice-Hall, Inc., Englewood Cliffs, New Jersey, 1987.

Timo Saksala
Structural Mechanics, BEN, Tampere University
P.O. Box 600, FI-33101 Tampere
timo.saksala@tuni.fi